

# Towards physiological motion compensation for flexible needle interventions

Pedro Moreira, Momen Abayazid and Sarthak Misra

**Abstract**—Flexible bevel-tipped needle steering has been an active research topic since the last decade. However, most of the work presented so far performs flexible needle steering in static phantoms or non-static virtual environments. The insertion of flexible bevel-tipped needles into soft-tissue subjected to motion disturbances is still an open research problem. In this paper, we propose a flexible needle steering algorithm that is able to handle physiological motion disturbances. The system estimates the disturbance using the force information provided by a force sensor placed in contact with the soft-tissue. The system is evaluated through experiments steering a flexible needle towards a physical target into a moving soft-tissue phantom. Three experimental cases with motion disturbances based on clinical procedures in the lung, kidney and heart are used to assess the targeting error. The average targeting error of all 15 experimental trials is  $1.05 \pm 0.41\text{mm}$ . Our results demonstrate the ability of the proposed system to compensate for motion disturbances applied to the soft-tissue phantom.

## I. INTRODUCTION

Needle interventions are commonly used for localized drug delivery and tissue sample removal for diagnosis [1]. Misplacement of the needle tip may result in unsuccessful treatment or false diagnosis. Therefore, accurate needle tip placement is of utmost importance. Inaccurate needle tip placement can be caused by several factors, such as needle deflection, anatomical obstructions, tissue inhomogeneity and physiological processes.

Physiological motions, such as respiratory motion, normally result in target displacement and unexpected needle/tissue interaction forces, leading to errors in the needle tip placement. In procedures such as lung and kidney biopsies respiratory motion is a major source of disturbance [2]. During respiration, tumors in the lung and in the upper abdominal organs can move from 5mm to 30mm [3]. A long training period is required for surgeons to be able to cope with these physiological disturbances [4]. The common clinical practice is to instruct the patients to hold their breath during the needle insertion or to use breath-hold monitoring devices to calibrate the patient breathing frequency [3]. The accuracy of such procedures are highly dependent on the patient ability to hold breath. In some cases, the need to halt respiration also means that general anesthesia must be used, increasing the risks for the patient [5]. Several robotic devices for needle insertion were presented to assist clinicians

Pedro Moreira, Momen Abayazid and Sarthak Misra are affiliated with the Surgical Robotics Laboratory, Department of Biomechanical Engineering (MIRA-Institute for Biomedical Technology and Technical Medicine), University of Twente, The Netherlands. Sarthak Misra is also affiliated with the Department of Biomedical Engineering, University of Groningen and University Medical Center Groningen, The Netherlands. Email: {p.lopepdafrotamoreira; m.abayazid; s.misra}@utwente.nl

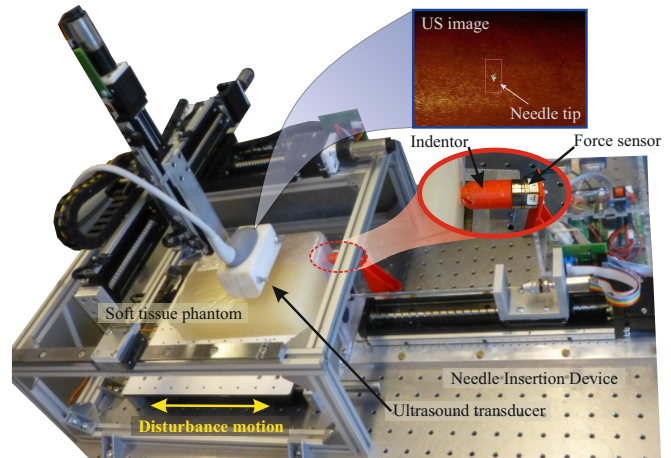


Fig. 1. The needle insertion device inserts and axially rotates a bevel-tipped flexible needle in a moving phantom. The needle tip is tracked by an ultrasound transducer controlled by a Cartesian robot. A 1 degree of freedom disturbance motion is applied to the soft-tissue phantom, and a force sensor is placed in contact with the soft-tissue phantom by an indentor. The measured force is used to estimate the disturbance motion.

during lung and kidney biopsies [6], [7]. A robot-assisted needle insertion device for lung biopsy was presented by Xu *et al.* [8]. The respiratory motion was tracked using computer tomography (CT) fluoroscopic images while a biopsy needle was inserted towards the target region. A different approach was proposed by Zhou *et al.* [4], where a conventional biopsy needle was inserted by a robotic device in one respiratory phase with an insertion speed of 500mm/s. Conventional biopsy needles are rigid, have limited steerability and the planned path is usually a straight line. Flexible and thin needles were introduced to facilitate curved paths, increasing the needle steerability. Such needles can be used to steer around sensitive and hard tissue such as blood vessels, nerves and bones. However, the use of flexible needles to reach a target in a moving tissue has not yet been investigated.

Flexible needles with a bevel tip naturally bend when inserted into soft-tissues. This bending effect can be used to robotically steer the needle towards a target using two degrees of freedom (needle insertion and axial rotation). In the last decade, many research groups have been working on the development of flexible needle steering systems [9]–[15]. Most of these works were designed to operate in static environments. Bernardes *et al.* [16] and Patil *et al.* [17] implemented an online path planner based on rapidly exploring random tree (RRT) in order to compensate for target and obstacle motions during flexible needle insertions.

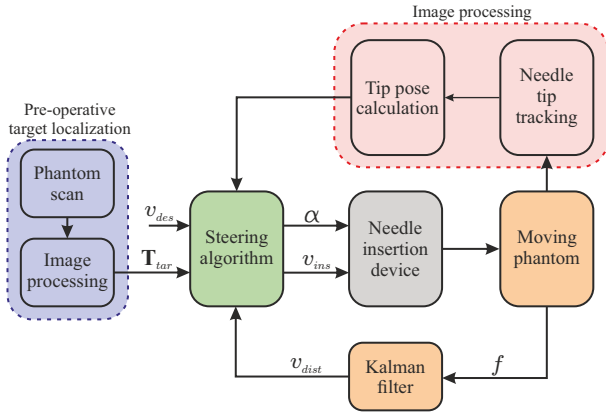


Fig. 2. The needle is inserted into a moving soft-tissue phantom by the needle insertion device. The needle insertion speed ( $v_{ins}$ ) and rotation angle ( $\alpha$ ) are defined by the steering algorithm. A Kalman filter is implemented in order to estimate the disturbance velocity ( $v_{dist}$ ) using the measured contact force ( $f$ ) as input. The insertion speed is controlled in order to keep the relative velocity between the needle base and the moving phantom at a desired velocity ( $v_{des}$ ). The needle rotation is defined using the target pose ( $\mathbf{T}_{tar}$ ) provided by the pre-operative target localization and the needle tip position given by the ultrasound image processing.

The desired needle path is recalculated every second based on the current needle tip, obstacle and target locations. The experimental results using ultrasound (US) feedback presented by Vrooijink *et al.* show that the RRT was able to handle the target motions [12]. However, the target motion addressed in these works were preplanned known motions, and were not based on clinical information of physiological motions. Moreover, the phantoms were static with virtual moving obstacles and targets (non-static virtual environment). Physiological disturbances can cause target motion but also induce forces on the needle tip, deviating the needle from its path. Therefore, it is important to evaluate the feasibility of performing flexible needle steering in a tissue with motion disturbances.

This work proposes a steering algorithm to perform flexible needle insertion in tissues subjected to physiological motions using force feedback and disturbance estimation (Fig. 1). The system is evaluated in three experimental cases. The flexible needle is steered towards a physical target in a soft-tissue phantom with different types of disturbance motions. The disturbances are defined based on clinical information of tissue displacement due to respiration and beating heart. To the best of the authors knowledge this is the first attempt to perform flexible needle steering in a moving soft-tissue phantom.

The paper is organized as follows. In Section II, the US-based needle tracking, the target localization, the steering algorithm and the physiological motion compensation are described. Section III presents the experimental setup and results, followed by Section IV, which concludes and provides directions for future work.

## II. METHODS

This section introduces the methods used to steer the flexible needle in a moving phantom. The flowchart of

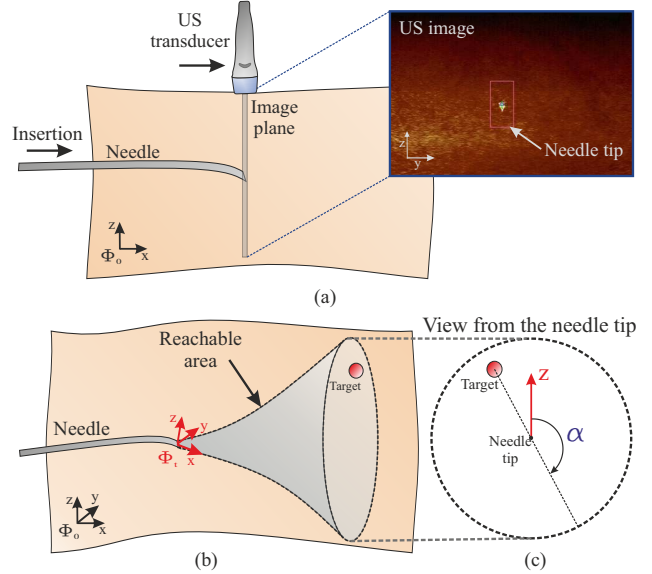


Fig. 3. (a) The needle is tracked by an ultrasound transducer placed perpendicular to the needle insertion axis. The ultrasound transducer position is controlled to keep the needle tip always in the image plane. The tracking algorithm provides the needle tip pose (position and orientation) in the initial reference frame ( $\Phi_0$ ). (b) The needle tip is assumed to follow a circular path in the direction of the bevel tip. The needle reachable area is defined by the needle curvature. (c) The steering algorithm computes the rotation angle ( $\alpha$ ) required to align the z-axis of the needle tip frame ( $\Phi_t$ ) to the target location.

the system is depicted in Fig. 2. The US-based needle tracking, the target detection and the steering algorithm are described in this section. The method used to compensate for physiological motion is also presented.

### A. Ultrasound-based needle tracking

The needle tip position and orientation are used as feedback for the needle steering control algorithm. We use a 2D US transducer to track the needle tip in 3D space. A Cartesian robot is used to control the US transducer position. The transducer is placed perpendicular to the needle insertion axis to visualize the cross-sectional view of the needle tip, as shown in Fig. 3a. Basic image processing techniques such as median filtering, thresholding, erosion and dilation are applied to localize the tip position in the US image frame. The y- and z- coordinates of the needle tip are obtained from the US image while the x-coordinate is obtained from the Cartesian robot controlling the US transducer. The needle tracking runs every 40 ms and the maximum errors in the estimated needle tip positions are 0.64 mm, 0.25 mm and 0.27 mm along the x-, y- and z-axes, respectively. Further details concerning the 3D needle tracking algorithm are presented by Vrooijink *et al.* [12].

### B. Pre-operative target localization

A pre-operative scan is performed to localize the target position inside the soft-tissue phantom. The robot controlling the transducer scans the phantom in steps of 0.4 mm to obtain the ultrasound image frames and their corresponding

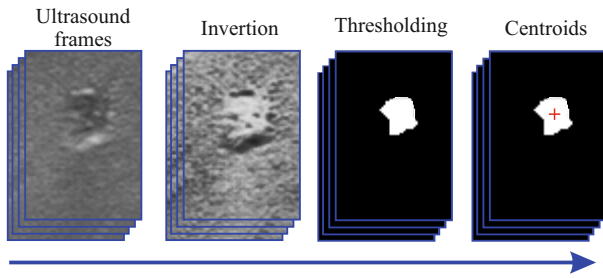


Fig. 4. The target location is determined by a pre-operative scan. The ultrasound image frames are inverted and then converted to binary images. The algorithm calculates the centroid of each cross-section of the target and the average of all centroids is considered as the target location.

transducer positions. The image frames are processed offline to localize the target. Each image frame is converted to a binary image based on a threshold value and the centroid of each cross-section of the target is obtained Fig. 4. The centroid location of the 3D volume is the average of all cross-section centroids. During the target localization scan, no disturbance motions are applied to the phantom. The entire target localization procedure takes an average of 6 minutes. The target location is used as input for the steering algorithm.

### C. Flexible needle steering algorithm

The steering algorithm uses the current needle tip pose provided by the US-based needle tracking and the current target pose to define the needle rotation around the x-axis required to reach the target. The needle is assumed to move along a circular path [18] and the direction of the circular motion depends on the needle tip orientation. The needle shaft follows the needle tip [9]. The needle tip initially moves in the direction of the negative z-axis of the needle tip frame ( $\Phi_t$ ). The steering algorithm computes every 40ms the rotation angle ( $\alpha$ ) required to align the z-axis of the needle tip orientation with the target position (Fig. 3). The insertion ends when the needle tip position and the target positions in the x-axis are equal.

The target pose with respect to the needle tip ( $\mathbf{T}_{tar}^{tip}$ ) is calculated using the needle tip pose in the initial reference frame ( $\mathbf{T}_{tip}^0$ ). The target pose with respect to the needle tip ( $\mathbf{T}_{tar}^{tip}$ ) is given by

$$\mathbf{T}_{tar}^{tip}(k) = (\mathbf{T}_{tip}^0(k))^{-1} \mathbf{T}_{tar}^0(k) \quad (1)$$

where  $\mathbf{T}_{tar}^0$  is the target pose in the initial reference frame ( $\Phi_0$ ) and  $k$  is the discrete index. The angle  $\alpha$  is determined by

$$\alpha(k) = \arctan\left(y_{tar}^{tip}(k), z_{tar}^{tip}(k)\right) + \frac{\pi}{2} \quad (2)$$

where  $y_{tar}^{tip}$  and  $z_{tar}^{tip}$  are the target coordinates in the needle tip frame. The addition of  $\frac{\pi}{2}$  is due to the definition of the needle tip frame where  $0^\circ$  is aligned with the negative y-axis.

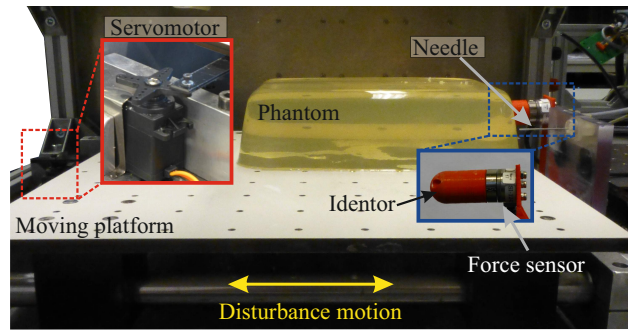


Fig. 5. A moving platform with one degree of freedom is implemented to provide physiological motions to the soft-tissue phantom. The platform is actuated by a servomotor which provides disturbance motion in the same direction as the needle insertion axis. The force sensor used to estimate the disturbance motion is placed next to the needle entry point.

### D. Physiological motion compensation

Tissue motion induced by physiological processes is a major issue in certain medical procedures, such as kidney and lung biopsies. The two main sources of disturbances are respiration and beating heart. Respiratory motions induce low frequency disturbances with large displacements. The breathing frequency for a healthy human usually varies between 0.1Hz and 0.4Hz, while the amplitude can be up to 30mm depending on the patient. Nodule displacement in lung biopsies is reported to vary from 10mm to 30mm and this displacement mainly occurs in the insertion direction [4]. The amount of disturbance induced by respiration depends on the proximity of the target area to the lung. In kidney biopsies, the induced target displacement due to respiration can vary from 4.5mm to 9.8mm [19]. On the other hand, disturbances induced by beating heart are usually significantly smaller than the one induced by respiration, ranging from 0mm to 3mm [20]. A Fourier analysis of the beating heart motion shows that several harmonics are present and the principal component is usually between 1Hz and 1.25Hz [21].

A moving platform is implemented in order to provide different physiological motions to the soft-tissue phantom during the needle insertion. The platform has 1 degree of freedom and can provide motions up to 20mm of amplitude and 1.5Hz of frequency, which can mimic disturbances due to breathing and beating heart according to the values reported in the literature. The phantom moves in the same axis as the needle insertion, as depicted in Fig. 5. The platform is actuated using a servomotor (MG995, TowerPro, Taiwan) and the disturbance motion profile is pre-loaded in a microcontroller board (Arduino Nano V3, Arduino, Italy), which controls the servomotor.

A force sensor (ATI Nano-17, Industrial Automation, USA) is placed next to the insertion point in a way that is always in contact with the soft-tissue phantom. In the current implementation, the force sensor location does not affect the disturbance estimation, since the disturbance motion is along the insertion direction. The measured force ( $f$ ) is used as an input in a Kalman Filter to estimate the disturbance position ( $p_{dist}$ ) and its velocity ( $v_{dist}$ ). The Kalman filter states are

given by  $\mathbf{z} = \begin{bmatrix} p_{dist} \\ v_{dist} \end{bmatrix}$  and the disturbance is modeled as

$$\mathbf{z}(k+1) = \begin{bmatrix} p_{dist}(k+1) \\ v_{dist}(k+1) \end{bmatrix} = \begin{bmatrix} 1 & \Delta T \\ 0 & 1 \end{bmatrix} \mathbf{z}(k) \quad (3)$$

where  $\Delta T$  is the time period of 40ms. The disturbance estimation is then given by

$$\hat{\mathbf{z}}(k+1) = \begin{bmatrix} 1 & \Delta T \\ 0 & 1 \end{bmatrix} \hat{\mathbf{z}}(k) + \mathbf{K}(k) \left( \frac{f(k)}{k_e} - \hat{p}_{dist}(k) \right) \quad (4)$$

where  $k_e$  is the phantom stiffness estimated prior the needle insertions and  $f(k)$  is the measured force. Using the stiffness instead of Young's modulus allows us to correlate the exerted force to the disturbance motion with only one parameter. The matrix  $\mathbf{K}(k)$  is the Kalman gain. The Kalman filter is experimentally tuned with measurement noise covariance equal to 0.1 and the system noise covariance is a  $2 \times 2$  diagonal matrix with elements equal to 0.001.

The estimated disturbance position ( $\hat{p}_{dist}$ ) and velocity ( $\hat{v}_{dist}$ ) are used to correct the target location ( $\mathbf{T}_{tar}$ ) and the insertion velocity ( $v_{ins}$ ), respectively. The needle insertion velocity is varied in order to keep a constant desired relative velocity ( $v_{des}$ ) between the needle base and the phantom. The steering algorithm changes the insertion velocity as

$$v_{ins}(k) = v_{des}(k) - \hat{v}_{dist}(k). \quad (5)$$

The x-coordinate of the target location is updated online as

$$x_{tar}(k) = x_{tar}(0) + \hat{p}_{dist}(k) \quad (6)$$

where  $x_{tar}(0)$  is the x-coordinate of the initial target pose ( $\mathbf{T}_{tar}^0(0)$ ) defined by the pre-operative target localization. The updated target pose is used by the steering algorithm to calculate the needle rotation in equations (1) and (2).

### III. EXPERIMENTS

In this section, we present the setup and the experimental plan used to evaluate flexible needle steering in a moving soft-tissue phantom. The experimental results and discussion are also presented.

#### A. Experimental setup

The experimental setup used to steer the needles into the soft-tissue phantoms is shown in Fig. 1. The needle insertion device has two degrees of freedom: translation along and rotation about the insertion axis. During the needle insertion, an US transducer (Transducer 18L6HD, Siemens ACUSON S2000 ultrasound system, Siemens AG, Germany) is used to estimate the needle tip pose. The needle used in the experiments is a 0.5mm diameter Nitinol needle with a bevel tip angle of  $30^\circ$ . The soft-tissue phantoms are prepared with a mixture of 84% of water, 15% of gelatin (Dr.Oetker, The Netherlands), and 1% of silica gel 63 (E. Merck, Germany). The silica gel is added to simulate the acoustic scattering

of human tissues in US images. The phantom stiffness ( $k_e$ ) for this mixture is 412N/m. The stiffness is estimated using the displacement and the exerted force measured in five tests compressing the phantom. The physical targets are embedded in the soft-tissue phantom while the gelatin is still liquid. The targets are spheres with 1.5mm radius made of Polyvinyl chloride (PVC). The target deformation is assumed to be negligible.

#### B. Experimental plan

Different experimental cases are conducted to validate the flexible needle steering in moving soft-tissue phantoms. The experimental cases are defined considering clinical procedures in the kidney, the lung and the heart. The amplitude and frequency of the movements applied to the soft-tissue phantom are based on characteristics of clinical procedures in these organs:

- Case 1: The phantom motion is defined in order to represent the kidney displacement during needle interventions. Using the values reported in the literature, the phantom movement is defined as a 0.2Hz sinusoidal motion with 7mm of amplitude.
- Case 2: The phantom motion is defined to mimic the lung displacement due to respiratory motion during needle interventions. The movement is a 0.2Hz sinusoidal motion with amplitude of 15mm. This experimental case is performed to test the ability of the system to steer the needle in tissues subjected to a respiratory motion.
- Case 3: The phantom motion is defined in order to simulate the beating heart displacement. The applied movement is a 1Hz sinusoidal motion with amplitude of 3mm. This experimental case is performed to test the feasibility of steering the needle in tissues subjected to a smaller and faster disturbance than Case 1 and 2.

The distance between the needle entry point and the target location randomly varies between 65mm and 79mm depending on the experimental trial. These three experimental cases allow us to assess the system ability to compensate for motion disturbances with different amplitudes and frequencies.

#### C. Experimental results

Five needle insertions are performed for each experimental case, in a total of 15 trials. The needle is inserted with a desired velocity  $v_{des} = 1\text{mm/s}$ . The targeting error is defined by the Euclidean distance between the last needle tip position and the target location. Table I summarizes the targeting error for all three experimental cases. In Case 1, where the displacement represent the kidney motion due to respiration, the average targeting error is  $1.10 \pm 0.43\text{mm}$ . The average targeting error for Case 2 is  $1.24 \pm 0.25\text{mm}$  and for Case 3 is  $0.80 \pm 0.45\text{mm}$ . The paths performed by the needle in three representative trials (one for each experimental case) are presented in Fig. 6. *Please refer to the accompanying video that demonstrates the experimental results.* A representative result of the disturbance estimation for all three experimental cases are presented in Fig. 7. It is possible to observe in Fig. 7 that the applied disturbances are

TABLE I

AVERAGE TARGETING ERROR AND STANDARD DEVIATION FOR ALL THREE EXPERIMENTAL CASES. THE TARGETING ERROR IS DEFINED AS THE EUCLIDEAN DISTANCE BETWEEN THE LAST NEEDLE TIP POSITION AND THE TARGET CENTROID.

	Targeting error	Standard deviation
Case 1	1.10mm	0.43mm
Case 2	1.24mm	0.25mm
Case 3	0.80mm	0.45mm

not a perfect sinusoidal motion due to friction and backlash in the servomotor.

#### D. Discussion

The results of Case 1 and Case 2 show that the system is able to handle disturbances with different amplitudes while keeping similar targeting accuracies. The amplitude of the disturbance in Case 2 is two times larger than that of Case 1, but the average targeting error is only 12% larger. Although the disturbance frequency of Case 3 is five times higher than in Case 1 and 2, the accuracy of Case 3 is slightly lower than Case 1 and 2. This happens because the disturbance amplitude is smaller, which suggests that the amplitude is a disturbance characteristic more relevant than the frequency. Considering the three cases, the average targeting error of all 15 trials is  $1.05 \pm 0.41$ mm, which is in the same range of the targeting error of flexible needle steering into static phantoms [17]. The experimental results prove the feasibility of using flexible needles to perform insertions with physiological motion compensation.

In the current study, the experimental setup is a simplified representation of clinical situations where physiological motion disturbance is an issue. In the experiments presented in this work, the target motion has a linear relationship with the motion at the soft-tissue phantom surface in contact with the force sensor. However, in some percutaneous needle intervention, target motions due to physiological processes might not be the same as the motion at the needle entry surface. In these cases it is possible to combine the current work with a system to track moving targets in order to guarantee a proper targeting accuracy.

#### IV. CONCLUSION

This work demonstrates a bevel-tipped flexible needle steering method for procedures in tissues subjected to motion disturbances. We propose a control algorithm to steer the needle using a disturbance estimation based on force measurements to compensate for physiological motions. The motions applied to the soft-tissue phantom are based on the disturbances present in clinical procedures in the kidney, lung and beating heart. The system has proved to be able to compensate for physiological motion disturbances in all three experimental cases. Although the amplitude and frequency of the applied disturbances vary, the system is able to keep the targeting error lower than 1.5mm in all 15 experimental trials. The three experimental cases present similar targeting error average, which demonstrates the ability of the system to

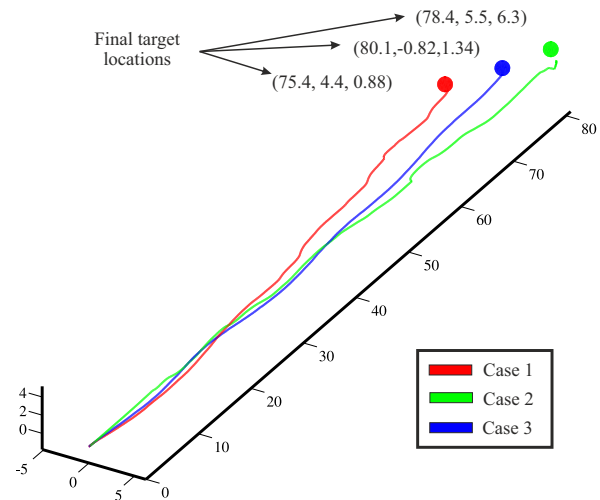


Fig. 6. Representative experimental results of steering a bevel-tipped flexible needle towards a physical target in a moving soft-tissue phantom. Red line is the path performed by the needle in Case 1, where the disturbance motion is based on kidney motion. Green line is one experimental result of Case 2, where the soft-tissue motion represents respiratory disturbances in lung interventions. Blue line is the result of Case 3, where the soft-tissue phantom movement is based on beating heart motion. Please refer to the accompanying video that demonstrates the experimental results.

handle different types of disturbances. The average targeting error of all experimental trials is  $1.05 \pm 0.41$ mm.

Future work will focus on the development of a new needle insertion device with two more degrees of freedom [22]. The force sensor will be attached directly to the end-effector of this new device and a force/torque control will be implemented to compensate for not only translational motion disturbances but also angular disturbances. The effect of different insertion velocities in the targeting accuracy will be studied. The use of accelerometers to improve the disturbance estimation will also be investigated. The accelerometer has to be placed on the soft-tissue phantom and will be used to correct for estimation errors due to slipping and friction forces in the force sensor contact point. We are also improving the moving platform to include disturbances in more degrees of freedom. Our study presents the preliminary results to validate the use of flexible needles in soft-tissues subjected to physiological disturbances such as respiratory and beating heart motions.

#### ACKNOWLEDGMENT

This research was supported by funds from the Dutch Ministry of Economic Affairs and the Provinces of Overijssel and Gelderland, within the Pieken in de Delta (PIDON) Initiative, Project MIRIAM (Minimally Invasive Robotics In An MRI environment).

#### REFERENCES

- [1] N. Abolhassani, R. Patel, and M. Moallem, "Needle insertion into soft tissue: A survey," *Medical Engineering Physics*, vol. 29, no. 4, pp. 413–431, 2007.

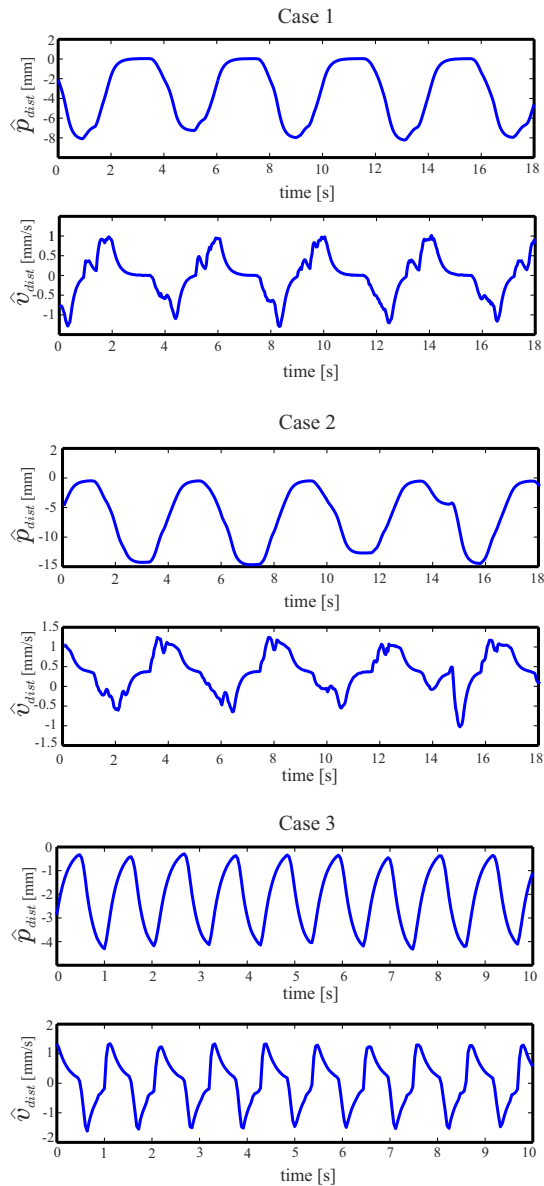


Fig. 7. Disturbance estimation of one representative trial of each experimental case. In Case 1 the disturbance is based on the kidney motion, Case 2 the disturbance is based on lung motion and Case 3 the disturbance is based on the beating heart motion. The top plots are the estimated disturbance position ( $\hat{p}_{dist}$ ) and the bottom plots are the estimated disturbance velocity ( $\hat{v}_{dist}$ ).

[2] S. K. Carlson, J. P. Felmlee, C. E. Bender, R. L. Ehman, K. L. Classic, H. H. Hu, and T. L. Hoskin, "Intermittent-mode CT fluoroscopy-guided biopsy of the lung or upper abdomen with breath-hold monitoring and feedback: System development and feasibility," *Radiology*, vol. 229, no. 3, pp. 906–912, 2003.

[3] C. R. Ramsey, D. Scapertho, D. Arwood, and A. L. Oliver, "Clinical efficacy of respiratory gated conformal radiation therapy," *Medical Dosimetry*, vol. 24, no. 2, pp. 115–119, 1999.

[4] Y. Zhou, K. Thiruvalluvan, L. Krzeminski, W. H. Moore, Z. Xu, and Z. Liang, "CT-guided robotic needle biopsy of lung nodules with respiratory motion experimental system and preliminary test," *The International Journal of Medical Robotics and Computer Assisted Surgery*, vol. 9, no. 3, pp. 317–330, 2013.

[5] C. N. Riviere, A. Thakral, I. I. Iordachita, G. Mitroi, and D. Stoianovici, "Predicting respiratory motion for active canceling during percutaneous needle insertion," in *Proceedings of the 23rd*

*Annual International Conference of the IEEE Engineering in Medicine and Biology Society*, vol. 4, 2001, pp. 3477–3480.

[6] J. Ding, D. Stoianovici, D. Petrisor, P. Mozer, R. Avila, L. Ibanez, W. Turner, D. Yankelvit, E. Wilson, F. Banovac, and K. Cleary, "Medical needle steering for lung biopsy: Experimental results in tissue phantoms using a robotic needle driver," in *Proceedings of the 8th IEEE International Conference on Bioinformatics and BioEngineering (BIBE)*, Athens, Greece, October 2008, pp. 1–5.

[7] L. B. Kratchman, M. M. Rahman, J. R. Saunders, P. J. Swaney, and R. J. Webster III, "Toward robotic needle steering in lung biopsy: a tendon-actuated approach," in *Proceedings of SPIE 7964, Medical Imaging 2011: Visualization, Image-Guided Procedures, and Modeling*, Lake Buena Vista, USA, 2011.

[8] S. Xu, G. Fichtinger, R. H. Taylor, F. Banovac, and K. Cleary, "CT fluoroscopy-guided robotically-assisted lung biopsy," in *Proceedings of SPIE 6141, Medical Imaging: Visualization, Image-Guided Procedures, and Display*, San Diego, USA, 2006.

[9] R. J. Webster III, J. S. Kim, N. J. Cowan, G. S. Chirikjian, and A. M. Okamura, "Nonholonomic modeling of needle steering," *The International Journal of Robotics Research*, vol. 25, no. 5-6, pp. 509–525, 2006.

[10] J. A. Engh, G. Podnar, D. Kondziolka, and C. N. Riviere, "Toward effective needle steering in brain tissue," in *Proceedings of the Annual International Conference of the IEEE Engineering in Medicine and Biology Society (EMBC)*, New York, USA, August 2006, pp. 559–562.

[11] D. S. Minhas, J. A. Engh, M. M. Fenske, and C. N. Riviere, "Modeling of needle steering via duty-cycled spinning," in *Proceedings of the Annual International Conference of the IEEE Engineering in Medicine and Biology Society (EMBC)*, Buenos Aires, Argentina, August 2007, pp. 5432–5435.

[12] G. J. Vrooijink, M. Abayazid, S. Patil, R. Alterovitz, and S. Misra, "Needle path planning and steering in a three-dimensional non-static environment using two-dimensional ultrasound images," *International Journal of Robotics Research*, vol. 33, no. 10, pp. 1361–1374, 2014.

[13] N. A. Wood, K. Shahrour, M. C. Ost, and C. N. Riviere, "Needle steering system using duty-cycled rotation for percutaneous kidney access," in *Proceedings of the Annual International Conference of the IEEE Engineering in Medicine and Biology Society (EMBC)*, Buenos Aires, Argentina, September 2010, pp. 5432–5435.

[14] M. C. Bernardes, B. V. Adorno, P. Poignet, and G. A. Borges, "Semi-automatic needle steering system with robotic manipulator," in *Proceedings of the IEEE International Conference on Robotics and Automation (ICRA)*, St. Paul, USA, 2012, pp. 1595–1600.

[15] M. Abayazid, R. J. Roesthuis, R. Reilink, and S. Misra, "Integrating deflection models and image feedback for real-time flexible needle steering," *IEEE Transactions on Robotics*, vol. 29, no. 2, pp. 542–553, 2013.

[16] M. C. Bernardes, B. V. Adorno, P. Poignet, and G. A. Borges, "Robot-assisted automatic insertion of steerable needles with closed-loop imaging feedback and intraoperative trajectory replanning," *Mechatronics*, vol. 23, no. 6, pp. 630–645, 2013.

[17] S. Patil, J. Burgner, R. J. Webster III, and R. Alterovitz, "Needle steering in 3-D via rapid replanning," *IEEE Transactions on Robotics*, vol. 30, no. 4, pp. 853–864, August 2014.

[18] V. Kallem and N. J. Cowan, "Image-guided control of flexible beveltip needles," in *Proceedings of the IEEE International Conference on Robotics and Automation (ICRA)*, Rome, Italy, 2007, pp. 3015–3020.

[19] S. Siva, D. Pham, S. Gill, M. Bressel, K. Dang, T. Devereux, T. Kron, and F. Foroudi, "An analysis of respiratory induced kidney motion on four-dimensional computed tomography and its implications for stereotactic kidney radiotherapy," *Radiation Oncology*, vol. 8, no. 248, 2013.

[20] L. E. Solberg, I. Balasingham, E. Fosse, and P. K. Hol, "Heart-induced movements in the thorax as detected by MRI," in *arXiv:1405.6747v1 [physics.med-ph]*, May 2014, pp. 1–5.

[21] P. Moreira, C. Liu, N. Zemiti, and P. Poignet, "Beating heart motion compensation using active observers and disturbance estimation," in *Robot Control*, vol. 10, no. 1, 2012, pp. 741–746.

[22] N. Shahriari, E. Hekman, M. Oudkerk, and S. Misra, "Design and evaluation of a computed tomography CT-compatible needle insertion device using an electromagnetic tracking system and CT images (in press) doi:10.1007/s11548-015-1176-3," *International Journal of Computer Assisted Radiology and Surgery*, pp. 1–8, 2015.